Combined DRS–RS–EXAFS–XANES–TPR Study of Supported Chromium Catalysts

Bert M. Weckhuysen* and Robert A. Schoonheydt
Centrum voor Oppervlaktechemie en Katalyse, K. U. Leuven, Kardinaal Mercierlaan 92, B-3001 Heverlee, Belgium

Jih-Mirn Jehng and Israel E. Wachs
Zettlemoyer Center for Surface Studies, Department of Chemical Engineering, Lehigh University, Bethlehem, PA 18015, USA

Sung June Cho and Ryong Ryoo
Department of Chemistry and Center for Molecular Science, KAIST, Taeduk Science Town, Taejon, 305-701, Korea

Sjoerd Kijlstra and Eduard Poels
Laboratorium voor Chemische Technologie, Universiteit van Amsterdam, Nieuwe Achtergracht 166, 1018 WV Amsterdam, The Netherlands

The surface chemistry of supported chromium catalysts ($Cr/SiO_2 \cdot Al_2O_3$) has been systematically investigated as a function of the support composition (Si : Al ratio) and the Cr oxide loading by a combination of diffuse reflectance spectroscopy (DRS), Raman spectroscopy (RS), X-ray Absorption spectroscopy (EXAFS–XANES) and temperature-programmed reduction (TPR). Combination of all the obtained results by these characterization techniques leads to a uniform interpretation and general picture of surface Cr. On hydrated surfaces, the molecular structure of the Cr oxide species depends on the isoelectric point of the oxide support and the Cr loading: more polymerized Cr oxide species correspond to higher Cr loading and silica content of the support. After calcination, the Cr oxide species are anchored onto the surface by reaction with surface hydroxy groups of the supports. On alumina the reaction starts with the most basic OH groups on alumina. This suggests that the anchoring process is an acid–base reaction. On calcined surfaces, the polymerization of the anchored Cr oxide species and the amount of Cr_2O_3 clusters increases with silica content and Cr loading. Reduced Cr samples possess both Cr^{2+} and Cr^{3+}, the relative concentrations of which are support and loading dependent: lower $Cr^{2+} : Cr^{3+}$ ratios correspond to higher Cr loading and alumina content of the support.

Knowledge of the surface chemistry of Cr oxide as a function of the support composition, chromium loading and environmental conditions is of key importance to understanding the behaviour of supported chromium catalysts.[1] Up to now, the identification of the molecular structures of surface Cr species remains controversial because of the lack of agreement in the literature between the results (*e.g.* chromate *vs.* dichromate) obtained by different techniques, such as diffuse reflectance spectroscopy (DRS), Raman spectroscopy (RS), thermogravimetry (TG) and infrared spectroscopy (IR).[2–17] Possible reasons for these different observations and interpretations might be: (1) differences in sensitivies of different techniques towards the nature of the surface Cr species; (2) differences in preparation and pretreatment of samples from different labs, even if they appear similarly prepared and pretreated. It is only by studying identical samples with different techniques that these controversial issues can be resolved.

In previous studies, we have developed a combined electron paramagnetic resonance–diffuse reflectance spectroscopy (EPR–DRS) method for the quantitation of Cr^{n+} (with $n = 2$, 3, 5 and 6) on inorganic oxides, at least at low Cr loadings.[18–23] The hydrated and calcined samples are loaded with chromate-like and dichromate-like species, the ratio of dichromate to chromate increasing from zero for Al_2O_3 to 1.39 for SiO_2 with intermediate values for silica aluminas, all with 0.2 wt.% loading of Cr (ref. 19).

At higher loadings the DRS–EPR techniques can only be applied qualitatively and other techniques must be introduced, especially those which give more detailed information at loadings above 0.4 wt.% Cr. These techniques are Raman spectroscopy (RS), extended X-ray absorption fine structure

(EXAFS), X-ray absorption near-edge structure (XANES) and temperature-programmed reduction (TPR). The objective of this study is twofold: (1) to solve the discrepancies in the literature about the molecular structure of Cr by a combination of several characterization techniques on the same set of samples, and (2) to study supported Cr at higher loading, which allows these results to be linked to our previous results.

Experimental

Sample Preparation and Characteristics

The supports (SiO_2, $SiO_2 \cdot Al_2O_3$ with 20, 40 and 60 wt.% SiO_2 and Al_2O_3) were homemade, the preparation methods being published elsewhere.[18,19] Nitrogen adsorption/desorption isotherms of the supports at 77 K were recorded on an Omnisorp 100 Analyzer from Coulter, operating in the continuous gas introduction and continuous pressure monitoring mode. The samples were pretreated *in vacuo* at 200 °C for 8 h. Surface areas and microporosity of the supports were derived from the measured isotherms using the BET method and the *t*-plot method, respectively. They are given in Table 1. The isoelectric point (IEP) values of the supports were determined by a method reported elsewhere[7] and the obtained values are included in Table 1. Chromium oxide supported catalysts were prepared by the incipient wetness technique with aqueous CrO_3. Amounts of solutions of CrO_3 equal to the pore volumes were mixed with the support under continuous stirring for 0.5 h. The concentration of Cr in the solution was adapted so as to obtain the desired loading. The

Table 1 Characteristics and preparation methods of the Cr-supported catalysts

support	BET surface area/$m^2 g^{-1}$	pore volume/ml g^{-1}	pore size/nm	IEP (pH)
Al_2O_3	365	2.0	3–9	8
$SiO_2 \cdot Al_2O_3$ with 20 wt.% SiO_2	337	1.7	1.5–8	5
$SiO_2 \cdot Al_2O_3$ with 40 wt.% SiO_2	329	1.4	1.5–7	4
$SiO_2 \cdot Al_2O_3$ with 60 wt.% SiO_2	253	1.0	1.5–10	3
SiO_2	735	0.8	1–3	2

Cr contents were determined by atomic absorption spectrometry (AAS) after dissolution of known quantities of the sample in HF/H_2SO_4. AAS measurements were performed using an Instrumentation Laboratory apparatus with a nitrous oxide–acetylene flame. The light source was a hollow cathode lamp with a wavelength of 357.9 nm. The measured Cr contents were between 0.2 and 8.0 wt.%.

Pretreatments and Characterization Techniques

Diffuse Reflectance Spectroscopy

The prepared samples were granulated for diffuse reflectance spectroscopy (DRS) measurements and the size fraction of 0.25–0.4 mm was loaded in a quartz flow cell with a Suprasil window. The samples were subsequently dried at room temperature and at 90 °C during 16 h, calcined at 550 °C for 6 h in an oxygen stream and reduced with CO for 30 min at 400 °C. Spectra were taken of the hydrated, the calcined and some of the reduced samples. Diffuse reflectance spectra (DRS) were taken on a Varian Cary 5 UV–VIS–NIR spectrophotometer at room temperature. The spectra were recorded against a halon white reflectance standard in the range 2500–200 nm. The computer processing of the spectra consisted of the following steps: (1) subtraction of the baseline, (2) conversion to wavenumber, and (3) calculation of the Kubelka–Munk (KM) function.

Raman Spectroscopy

Raman spectra (RS) were taken with a Spex Triplemate 1877 spectrometer coupled to a Princeton Applied Research optical multichannel analyser (Model 1463) equipped with an intensified photodiode array detector (1024 pixels, cooled to 243 K) and with a Spectra Physics Model 171 Ar^+ laser tuned to the 514.5 nm line. The hydrated Raman spectra were obtained under ambient conditions with the sample rotating at ca. 2000 rpm, while Raman spectra of the dehydrated samples (after calcination at 400 °C in oxygen for 2 h) were collected with an in situ cell that contained a stationary sample.

EXAFS–XANES

The investigated samples were 4 wt.% Cr/SiO_2, 4 wt.% Cr/Al_2O_3 and 4 wt.% $Cr/SiO_2 \cdot Al_2O_3$ with 40 wt.% SiO_2. Each powder sample (0.10 g) was pressed into a self-supporting wafer, 10 mm in diameter. EXAFS and XANES of the sample wafer were measured in air at room temperature. For the measurements of the calcined samples, the sample wafers were placed in a Pyrex U-tube flow reactor that was joined with an EXAFS cell. The EXAFS cell was fabricated with Pyrex tubing, and Kapton windows (125 μm, DuPont) were attached to the EXAFS cell using Torr Seal (Varian). The sample in the reactor was heated from room temperature to 450 °C at a rate of 1.5 °C min^{-1} in an oxygen flow and the final temperature was maintained for 2 h. The reactor was filled with helium after subsequent outgassing of oxygen at

room temperature. This calcined sample wafer was transferred into the EXAFS cell by tilting the reactor. To avoid hydration of the sample, the EXAFS cell with the sample in helium was flame sealed and kept in a vacuum desiccator until the EXAFS was measured. For the measurement of reduced samples, the sample wafer was calcined in the same way as above and subsequently reduced for 30 min using CO flow at 400 °C. The CO gas was evacuated at room temperature and helium was introduced as above.

The X-ray absorption measurement was carried out above the Cr K-edge (5989 eV) using Beam Line 7C at the Photon Factory in Tsukuba (Japan). The injection beam energy was 2.5 GeV. The ring current was maintained as 250–350 mA during the measurements. An Si(111) double crystal monochromator was used. Typical resolution at the Cr edge ($\Delta E/E$) was 1.1×10^{-4}. A focusing double mirror was installed and the beam was detuned by 75% to remove higher harmonics. The energy steps in the absorption edge and EXAFS regions were 0.5 and 2.3 eV, respectively. The X-ray intensity was measured by using a gas ionization chamber. Detector gasses for the incident and transmitted X-ray intensities were 30% N_2–70% He and 100% N_2, respectively.

The analysis of the X-ray absorption data was carried out by standard methods using the UWXAFS2 codes distributed by the University of Washington.[24,25] The background in the EXAFS spectrum was removed by the method of Newville et al.[26] The EXAFS oscillations [$\chi(k)$] above the Cr K-edge were weighted by k^3 after converting energy to wavevector, k. The $k^3\chi(k)$ values in the range of 3–13 $Å^{-1}$ were Fourier transformed into the R-space with a Hanning window function of 1 $Å^{-1}$ at each side.[27] The curve fit of the theoretical EXAFS function to the experimental function was done in the R-space using the amplitude function and phase function generated from FEFF5.[25] X-Ray absorption data of the following substances were used as standards: K_2CrO_4, Cr_2O_3, $CrCl_3 \cdot 9H_2O$ and Cr_{foil}. Careful examination of the XANES spectra of the standards and the Cr samples revealed that the chemical environments in the hydrated and calcined Cr samples were very similar to that of the K_2CrO_4 standard. Curve-fitting of the theoretical EXAFS function of CrO_4^{2-} to the experimental EXAFS function in the R-space gave an amplitude reduction factor (S_0^2) equal to 0.63. This value and EXAFS function of CrO_4^{2-} were used for curve-fitting of the hydrated samples and the calcined samples. Similarly, an S_0^2 factor of 0.64 was obtained from Cr_2O_3 and the EXAFS function was used in the curve-fitting of the reduced Cr samples. The fit range in R-space was 0.7–3.5 Å. A maximum number of free-fitting parameters of 18 was obtained using the equation, $N_{free} = 2\delta k\delta R$, with N_{free} the number of free-fitting parameters, δk the range of k in Fourier transformation and δR the fitting range in R-space. Throughout the curve-fit, the number of fitting parameters was always smaller than the N_{free} values.

Temperature-programmed Reduction

Temperature-programmed reduction (TPR) experiments were performed on a homemade apparatus with a quartz reactor

connected with a thermal conductivity detector interfaced with an integrator. Heating was performed with a tubular furnace. The reducing gas was a mixture of N_2 and CO (1% CO), while for calcination 20% oxygen in nitrogen was used. The samples were subsequently dried at 100 °C for 1 h and calcined at 550 °C for 6 h. The heating rate was 2 °C min^{-1}. After calcination, the samples were reduced with CO at a heating rate of 1 °C min^{-1}. The flow rate of the individual gases was regulated by mass flow controllers. The sample amount in each TPR experiment was typically 100 mg. These amounts were corrected for their dry weight determined by thermogravimetrical analysis, performed with a TGA–DTA92 apparatus of Setaram.

Results

Combined Diffuse Reflectance–Raman Spectroscopies

The assignments of the observed bands can be made by considering the Raman and DRS bands of some relevant chromium oxide reference compounds which are published in the literature.[28] It is also important to notice that the colour of the samples reflects the presence of the majority species. Yellow is characteristic of monochromate, orange of dichromate (or polychromates), and the presence of Cr^{3+} is revealed by a greenish shade, while Cr^{2+} gives a blue colour to the material.

Hydrated Cr on Oxidic Surfaces

Typical Raman and DRS spectra of hydrated Cr on alumina are shown in Fig. 1. At small loadings, the samples are yellow and have RS bands centred at 865 and 360 cm^{-1}, while DRS shows absorptions at 27 200 and 36 700 cm^{-1}. These bands are typical for monochromate. An increase of the Cr loading results in yellow–orange samples and the formation of two new Raman bands at 220 and 900 cm^{-1} which become dominant at the highest Cr oxide loading (8.0 wt.%). These bands are typical for dichromate and this is confirmed in DRS by a high-frequency broadening of the 27 200 cm^{-1} band and the appearance of a shoulder at 23 000 cm^{-1}. The chromate → polychromate transition is seen at 8 wt.% Cr in DRS and at 4 wt.% Cr in RS, indicating that the latter technique is more sensitive to the presence of polychromate.

The RS and DRS spectra of hydrated Cr/SiO$_2$ are illustrated in Fig. 2. At the lowest loading, a single RS band at 895 cm^{-1} is apparent while the DRS spectra are dominated by two bands at 28 700 and 41 600 cm^{-1} and a shoulder at 23 300 cm^{-1}. These Raman and DRS bands are due to dichromate. Increasing the Cr loading results in a broadening of the DRS 28 700 cm^{-1} band towards 27 000 cm^{-1} and the 23 300 cm^{-1} shoulder becomes more important. RS shows the formation of surface trichromate and tetrachromate (380, 850, 900 and 960 cm^{-1}). Due to fluorescence problems the hydrated Cr/SiO$_2$·Al$_2$O$_3$ samples could not be measured with RS. The DRS spectra of these samples are intermediate between those of Cr/SiO$_2$ and Cr/Al$_2$O$_3$.

In both Fig. 1(b) and 2(b) it is observed that the intensities of the O → Cr^{6+} charge-transfer transitions do not increase linearly with loading over the full range investigated, especially for hydrated Cr/SiO$_2$ and for Cr/Al$_2$O$_3$ with 8 wt.% Cr. This is due to a combination of two factors: (a) the scattering power of the carriers is dependent on the Cr loading and (b), more importantly, as the Cr loading increases, the penetration depth of the light beam decreases, less particles are probed and the relative fraction of specularly reflected light increases. As a consequence, the intensity and the resolution decrease.
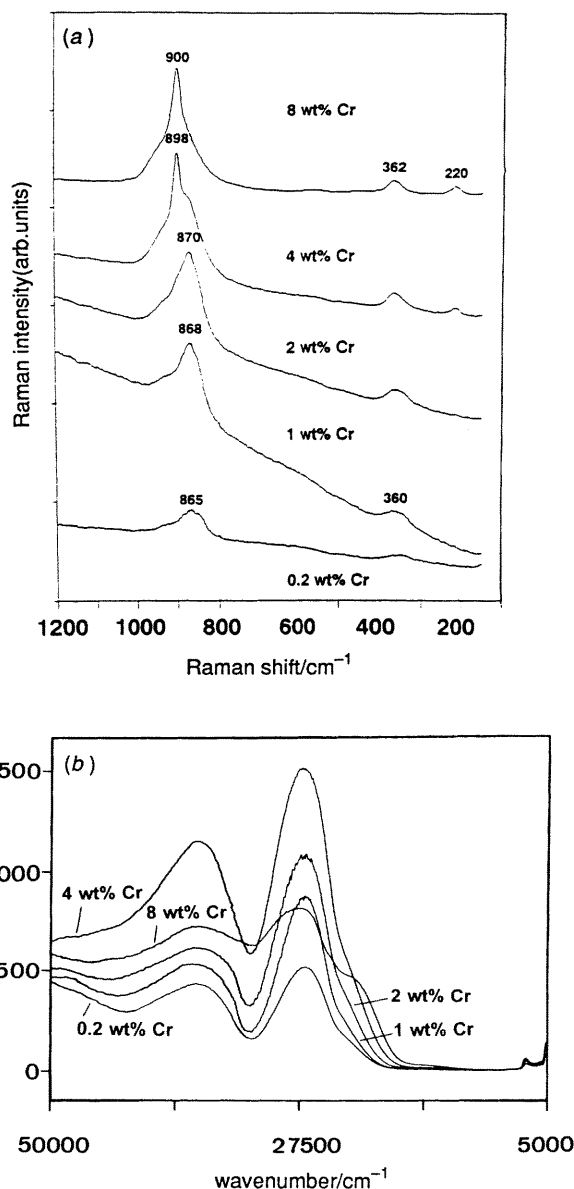

Fig. 1 Raman spectra (a) and DRS spectra (b) for increasing Cr loading of hydrated Cr/Al$_2$O$_3$ samples

Anchored Cr on Oxidic Surfaces

The calcined Cr samples possess a strong fluorescence background which prevents the collection of Raman spectra. The colour of the calcined Cr/Al$_2$O$_3$ samples changes from yellow over yellow–orange to dark orange with increasing Cr oxide loading. The DSR spectra, shown in Fig. 3, are typical for chromate for 0.2–4 wt.% Cr catalysts. Note that the second O → Cr^{6+} band around 40 000 cm^{-1} at 0.2 wt.% Cr shifts to 38 000 cm^{-1} at 4 wt.% Cr. As for the hydrated samples, the spectrum of the 8 wt.% Cr/Al$_2$O$_3$ is ill resolved owing to specular reflection and extends down to ca. 7000 cm^{-1}, which is indicative for the presence of some low-valent Cr. However, the broadening of the 27 200 cm^{-1} band and the formation of the 22 400 cm^{-1} band indicate the formation of polymeric Cr.

Fig. 4 shows the DRS spectra of calcined Cr/SiO$_2$ with increasing Cr loading. As for the hydrated samples, the spectra are typical mixed chromate–dichromate spectra. This is most clearly seen for 0.2 wt.% and 1 wt.% Cr samples with a two-component band in the region 30 000 (dichromate)–28 000 (chromate), shifting to 28 000 cm^{-1} for 4 wt.% Cr. The weak 15 000 cm^{-1} absorption, if present, is due to Cr^{3+}. As

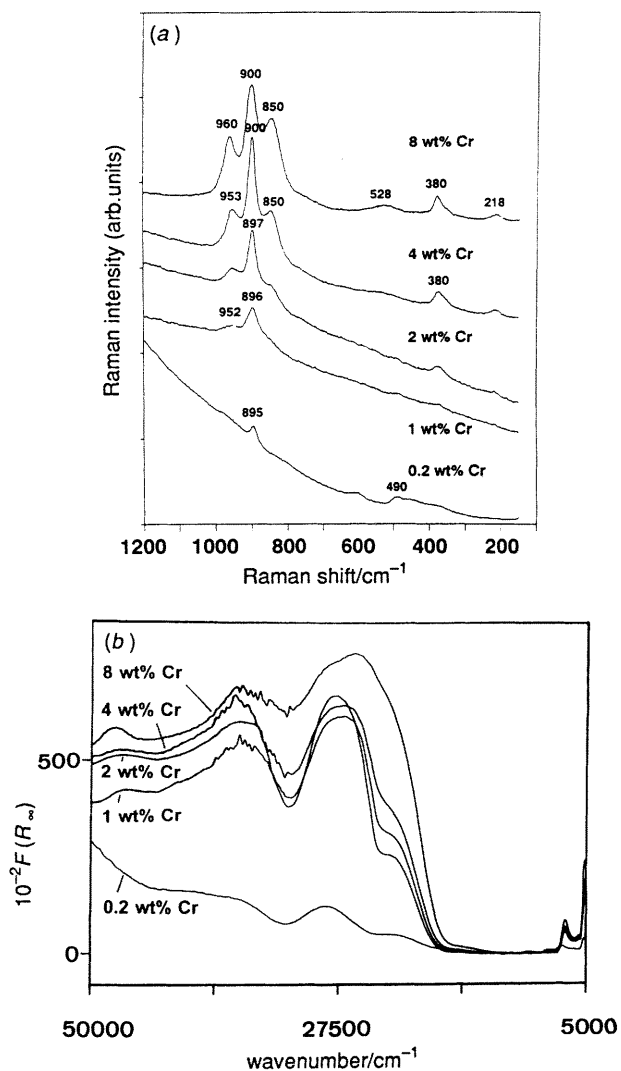Fig. 2 Raman spectra (a) and DRS spectra (b) for increasing Cr loading of hydrated Cr/SiO_2 samples
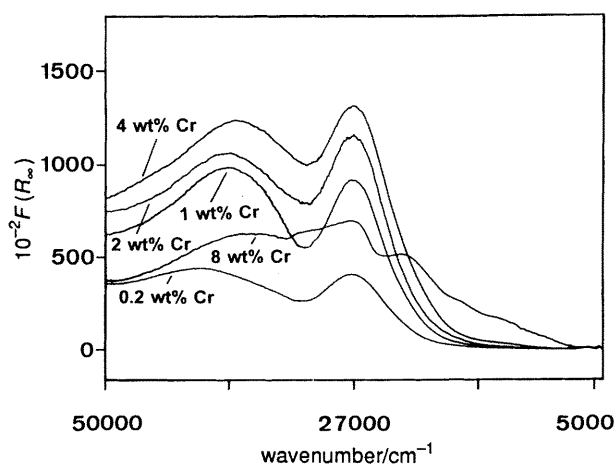

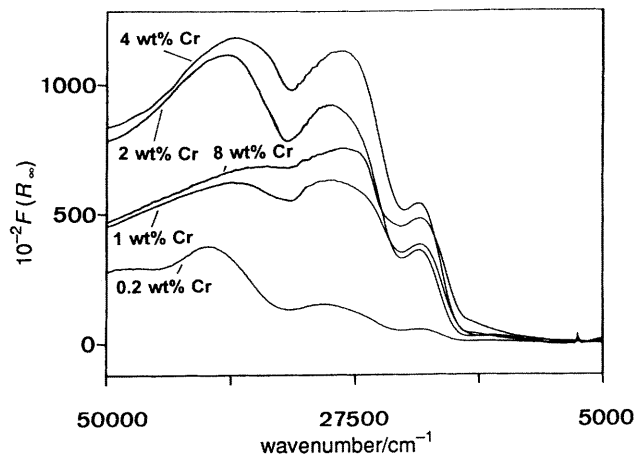Fig. 3 DRS spectra for increasing Cr loading of calcined Cr/Al_2O_3 samples

Fig. 4 DRS spectra for increasing Cr loading of calcined Cr/SiO_2 samples

overtone OH bands in the near-IR (NIR), as shown in Fig. 5. Alumina has a broad multicomponent band in the region 1350–1400 nm, while silica has a sharp OH band at 1366 nm. On all supports the OH band intensity decreases with increasing Cr loading, indicative of OH consumption. On alumina, the high-frequency OH groups are preferentially eliminated and two broad bands centred at *ca.* 1379 and 1399 nm remain at the highest Cr oxide loading. This shows that the most basic OH groups are preferentially eliminated. However, on all supports some residual OH groups remain. This may be due to the inaccessibility of these OH groups. Similar results on alumina were previously obtained by IR spectroscopy.[29]

Reduced Cr on Oxidic Surfaces

The DRS spectra of reduced Cr samples with low Cr loadings have been extensively studied in the past[10,14,18–21,30–32] and will not be repeated. The DRS spectra of high-loaded Cr/SiO_2 (blue–green) and Cr/Al_2O_3 samples (green) reduced with CO at 400 °C (not shown for brevity) possess always three bands of octahedral Cr^{3+}, while for silica surfaces additional bands at 7500 and 10000 cm^{-1} are observed. The latter two bands are due to (pseudo)tetrahedral and octahedral Cr^{2+}.[18,19] The silica–alumina samples display intermediate behaviour.

for 8 wt.% Cr/Al_2O_3, the 8 wt.% Cr/SiO_2 is ill-resolved owing to specular reflection. For the dehydrated $Cr/SiO_2 \cdot Al_2O_3$, intermediate spectra between those of alumina and silica are obtained.

The reaction between Cr oxide and the OH groups of the supports during calcination was monitored by recording the
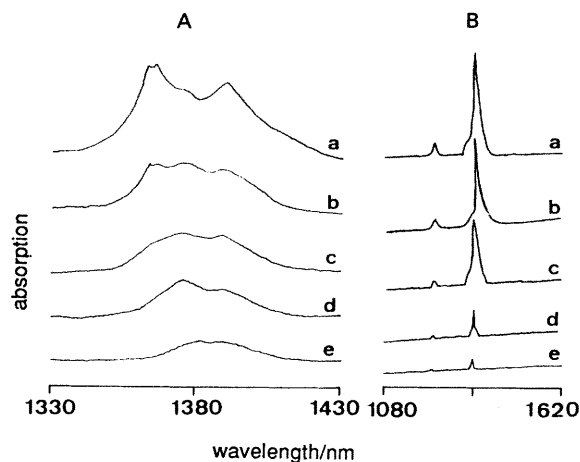

Fig. 5 Near-IR region of the DRS spectra of calcined Cr/Al_2O_3 (A) and Cr/SiO_2 (B) for increasing Cr loading: (a) 0.2 wt.%; (b) 1.0 wt.%; (c) 2.0 wt.%; (d) 4.0 wt.% and (e) 8.0 wt.%

Combined XANES–EXAFS Spectroscopies

XANES

Fig. 6 shows the near-edge spectra of Cr in the hydrated, calcined and reduced samples. In the hydrated samples, the sharp feature in the pre-edge region around 5992 eV is due to the dipole-forbidden transition 1s → 3d (ref. 33–35) and is characteristic of 3d metal oxides in tetrahedral coordination without an inversion centre.[34] The near-edge spectrum of K_2CrO_4 was suitable for curve-fitting of these Cr samples. The intensities of the sharp peak around 5992 eV change after calcination, indicating a change of symmetry around Cr or a slight distortion. After reduction of the samples, the sharp peak disappears. The near-edge feature changes dramatically and becomes similar to that of the Cr foil and Cr_2O_3 reference samples. The near-edge spectra of the reduced samples are shown in Fig. 7. The near-edge feature around 5995 eV is the strongest for Cr/SiO_2, while the spectra of Cr/Al_2O_3 and $Cr/SiO_2 \cdot Al_2O_3$ are quite similar. Consequently, the following order of reduction is inferred: $SiO_2 > SiO_2 \cdot Al_2O_3 > Al_2O_3$.

EXAFS

The Fourier transforms (FT) of the EXAFS spectra of hydrated, calcined and reduced Cr samples are shown in Fig. 8. For hydrated Cr/SiO_2, an FT peak is seen at ca. 1.3 Å with out-of-phase shift correction, which is split into two
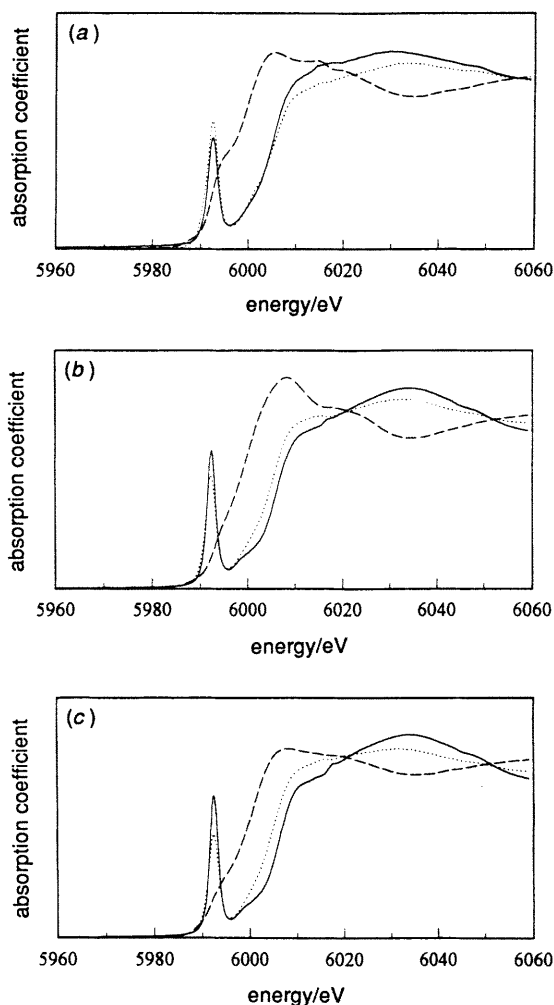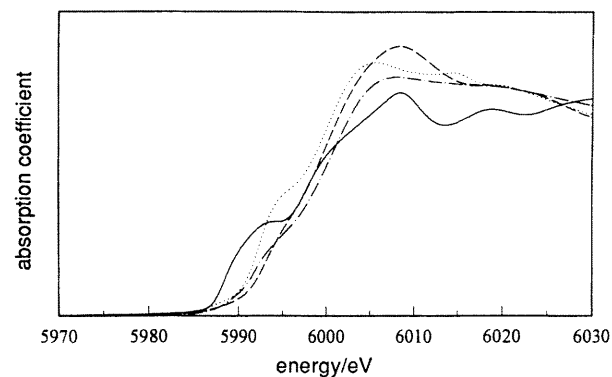

Fig. 7 Near-edge spectra of the reduced Cr/SiO_2 ($\cdots$), Cr/Al_2O_3 (–––), $Cr/SiO_2 \cdot Al_2O_3$ (– · –) and Cr foil (——)

peaks at ca. 1.1 and 1.6 Å after calcination. For the hydrated Cr/Al_2O_3 and $Cr/SiO_2 \cdot Al_2O_3$ (40 wt.% SiO_2) samples, an FT peak appears at ca. 1.3 Å as for hydrated Cr/SiO_2. When the samples are calcined, the peak intensity decreases by up to ca. 40% of the original intensity of the hydrated samples but without peak splitting. The FT peak intensity of the hydrated Cr/SiO_2 sample is smaller than that of the Cr/Al_2O_3 and $Cr/SiO_2 \cdot Al_2O_3$ samples. The peak intensity at ca. 1.3 Å reveals the numbers of oxygens around the Cr ion. This number is almost the same for the Cr/Al_2O_3 and $Cr/SiO_2 \cdot Al_2O_3$ samples, but lower for the calcined samples than for the hydrated ones. When the Cr samples are reduced, the peak at ca. 1.3 Å shifts to 1.6 Å and its intensity decreases further. This is indicative of structural changes.

The results of the curve-fitting of the spectra are summarized in Table 2, while the best curve-fitted EXAFS functions are shown as dotted lines in Fig. 8. For hydrated Cr/SiO_2, the Cr—O distance, the coordination number and the Debye–Waller factor for the first shell are 1.58 Å, 3.7 and 0.0041 Å^2, respectively, and are similar to those of the K_2CrO_4 reference sample ($N = 3.9$, $R = 1.62$ Å and $\sigma^2 = 0.0013$ Å^2), except for the Debye–Waller factor. For hydrated Cr/Al_2O_3 and $Cr/SiO_2 \cdot Al_2O_3$, the coordination number of Cr—O is close to 6 and the bond distance is 1.65 Å. The large value of N for Cr/Al_2O_3 and $Cr/SiO_2 \cdot Al_2O_3$ can be explained by a hydrated monochromate species, while lower N values are indicative of polymerized Cr. The bond distance of 1.65 Å indicates that all oxygens in the coordination sphere are in a bridge position or that coordinating water molecules make the Cr ion more relaxed by coordination, thus increasing the Debye–Waller factor. These results suggest that Cr on hydrated silica is a polymeric oxide (dimeric, trimeric, ...), while on alumina and silica–alumina, Cr is a hydrated monochromate species.

For calcined Cr/SiO_2, two Cr—O distances were observed at 1.53 and 2.05 Å with a similar coordination number N, ca. 2.1. Also, a Cr—Cr contribution was seen at rather short distance (3.1 Å) and with a higher coordination number, compared to those of hydrated Cr/SiO_2. A polychromate ion may be attached on the silica surface upon calcination. This attached polychromate possesses both bridging and terminal Cr atoms with two different Cr—O distances of 2.05 and 1.65 Å, respectively. An alternative interpretation is that the 1.53 Å distance is representative of polychromate, while the 2.05 Å distance reflects the presence of Cr^{3+} oxides. The latter interpretation is in line with the DRS data. The calcined Cr/Al_2O_3 and $Cr/SiO_2 \cdot Al_2O_3$ have no such change in Cr—O bond distance. The obtained coordination numbers of Cr—O are 3.4 for Cr/Al_2O_3 and 2.4 for $Cr/SiO_2 \cdot Al_2O_3$, respectively, indicating that on alumina and silica–alumina, Cr is monomeric.

Fig. 6 Near-edge spectra of the hydrated (——), calcined ($\cdots$) and reduced (–––) Cr samples: (a) Cr/SiO_2; (b) Cr/Al_2O_3 and (c) $Cr/SiO_2 \cdot Al_2O_3$
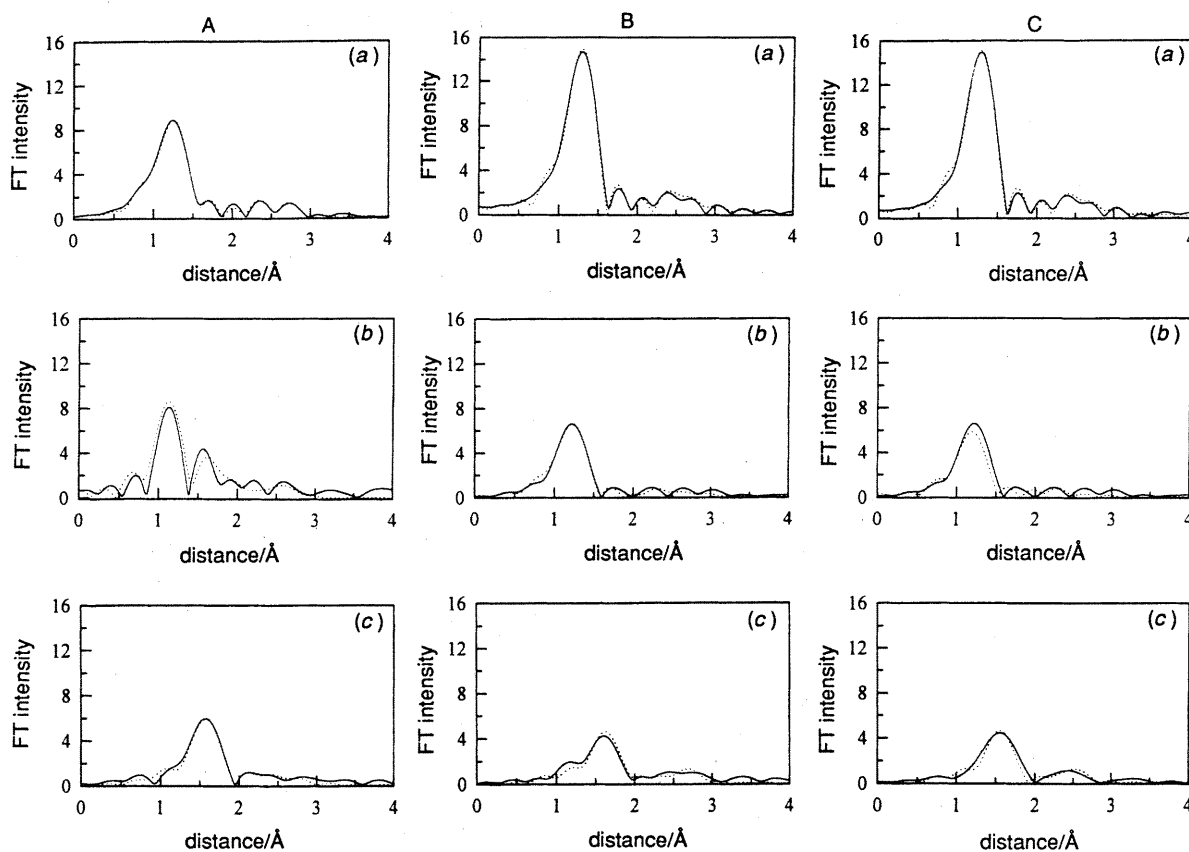
Fig. 8 Fourier transform of Cr K-edge EXAFS spectrum (solid line) for Cr/SiO$_2$ (A), Cr/Al$_2$O$_3$ (B) and Cr/SiO$_2$ · Al$_2$O$_3$ (C) and its best fitted theoretical EXAFS function in R-space (dotted line): (a) hydrated sample; (b) calcined sample and (c) reduced sample

By reduction, the Cr—O contribution at 1.6 Å disappears owing to a structural change of the anchored Cr. The Cr—O distances shift toward 2.0 Å with a small coordination number, while the Cr—Cr contribution is around 3 Å. The Cr—O distance of 2.0 Å is characteristic of oxides with lower valent Cr, such as Cr$_2$O$_3$. Thus, during reduction small clusters of supported Cr oxides are formed.

Temperature-programmed Reduction

As an example, the TPR profiles of Cr/Al$_2$O$_3$ for increasing Cr loading are shown in Fig. 9. Three observations can be made: (1) there is one TPR peak, which increases in intensity with increasing Cr loading; (2) the width of the TPR peak becomes broader, the lower the Cr loading; (3) the maximum

Table 2 Curve-fit results of the Cr K-edged EXAFS spectra of 4 wt.% Cr/SiO$_2$, Cr/Al$_2$O$_3$ and Cr/SiO$_2$ · Al$_2$O$_3$

Cr sample	pretreatment	atomic pair	N^a	R^b/Å	σ^2/Å$^{2\,c}$
Cr/SiO$_2$	hydrated	Cr—O	3.7	1.58	0.0041
		Cr—O—O^d	18.1	2.91	0.0041
		Cr—Cr	0.3	3.28	0.0013
	calcined	Cr—O	2.2	1.53	0.0013
		Cr—O	2.1	2.05	0.0024
		Cr—Cr	0.5	3.10	0.0030
	reduced	Cr—O	2.5	2.01	0.0030
		Cr—Cr	1.5	2.97	0.0121
Cr/Al$_2$O$_3$	hydrated	Cr—O	5.7	1.65	0.0038
		Cr—O—O^d	24.2	3.02	0.0038
	calcined	Cr—O	3.4	1.64	0.0053
		Cr—O—O^d	3.5	3.03	0.0053
	reduced	Cr—O	3.4	2.03	0.0031
		Cr—Cr	1.4	3.13	0.0108
Cr/SiO$_2$ · Al$_2$O$_3$	hydrated	Cr—O	5.8	1.65	0.0038
		Cr—O—O^d	24.1	3.02	0.0038
	calcined	Cr—O	2.4	1.64	0.0035
		Cr—O—O^d	8.5	2.85	0.0035
	reduced	Cr—O	2.4	2.01	0.0024
		Cr—Cr	0.7	2.98	0.0049

^{a} Coordination number; ^{b} bond distance; ^{c} the Debye–Waller factor; ^{d} forward and backward multiple scattering.
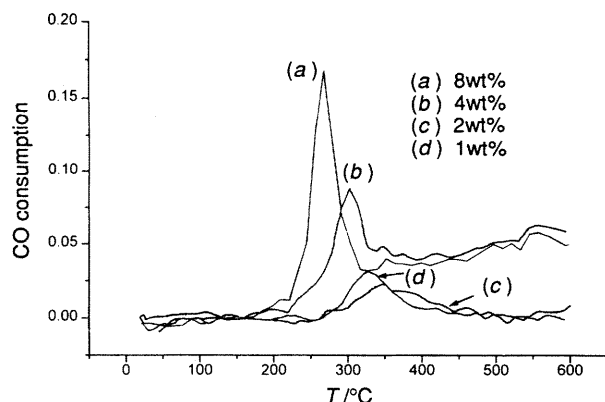
Fig. 9 TPR profiles of Cr/Al_2O_3 for increasing Cr loading

of the TPR peak shifts towards lower temperatures with increasing Cr loading (*i.e.* increasing amount of polymerized Cr^{6+}). The same observations are made for the other supports.

The TPR profiles, especially those of 4 and 8 wt.% Cr supported catalysts, possess a background of CO consumption above 450 °C, due to a water gas shift reaction:[36]

$$CO + 2X-OH \rightarrow CO_2 + H_2 + X-O-X \text{ (with } X = Si \text{ or } Al),$$
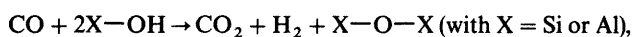
which complicates the quantification of the TPR profiles. The calculation of the mean oxidation state in each sample is derived from the area under the TPR peak and from the

Table 3 Mean oxidation state and temperature of maximum CO consumption for different Cr catalysts

$SiO_2 \cdot Al_2O_3$ with x wt.% SiO_2	Cr loading (wt.% Cr)	n in Cr^{n+}	temperature of maximum CO consumption/°C
0	1.0	2.7	364
	2.0	2.8	334
	4.0	3.0	303
	8.0	3.1	268
20	2.0	2.5	327
	4.0	2.7	304
40	2.0	2.3	336
	4.0	2.6	318
60	2.0	2.2	318
	4.0	2.3	284
100	1.0	1.5	354
	2.0	2.1	332
	4.0	2.2	299
	8.0	2.8	288

amount of Cr. The calculated mean oxidation states of Cr are summarized in Table 3, together with the temperature of maximum CO consumption.

For each support the average oxidation number of Cr decreases with decreasing loading. In addition, when the supports with the same Cr loading are compared, the average oxidation number of Cr decreases from alumina over silica–alumina to silica, an observation that is in line with the DRS data. Recently, similar TPR results were published for Cr/SiO_2 and Cr/Al_2O_3 catalysts by Fouad *et al.*[17]

Discussion

Evaluation of the Combination of Characterization Techniques

All the techniques used in this study give qualitative information on the oxidation state of Cr, its coordination environment and its degree of dispersion. However, the sensitivity of each technique to each of these three parameters is different.

Because of the very intense $O \rightarrow Cr^{6+}$ charge transfer (CT) transitions, DRS is very sensitive to the presence of chromate and polychromate. Loadings of $\leqslant 0.1$ wt.% can easily be detected. The technique is quantitative in this low loadings regime, but not at high loading for reasons discussed in this paper. Its disadvantage is that relatively large amounts of sample are needed (2 g). Cr^{2+} and Cr^{3+} have to be discerned *via* their d–d transitions. These are inherently much less intense than the CT transitions and, therefore, DRS is less sensitive towards these ions than towards Cr^{6+}.

Raman spectroscopy is always less sensitive towards Cr^{n+} than DRS and, from the experimental side, suffers from possible fluorescence problems, especially after calcination. The advantage of RS is that it is able to distinguish between the different forms of polychromate (dichromate, trichromate, ...) and monochromate.

EXAFS–XANES is not a sensitive technique as the minimum Cr loading needed is 2 wt.%. However, it provides accurate coordination distances and approximate coordination numbers. In that way EXAFS–XANES data complement the DRS data. Finally, the overall chemistry of the reduction process is revealed by TPR. The minimum loading needed is 1 wt.%. TPR gives data that are nicely complementary to the spectroscopic data. Indeed, the mean oxidation state of Cr revealed by spectroscopic techniques must be in agreement with those obtained by TPR.

All the techniques used in this paper were applied on samples with 4 wt.% Cr (Table 4) and a qualitative comparison is possible. There is agreement among the results of all the techniques that both on hydrated and calcined catalysts, monochromate is the dominant species on alumina and polychromates on silica. Only with RS has it been possible to identify unambiguously polychromate species on 4 wt.% Cr/Al_2O_3. Thus, Raman spectroscopy is the most sensitive

Table 4 Comparison of the obtained results on 4 wt.% Cr-loaded samples with different characterization techniques
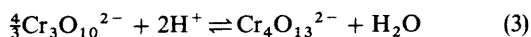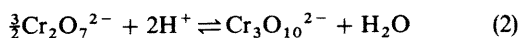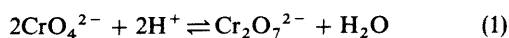
sample	treatment	DRS	RS	EXAFS–XANES	TPR
Cr/SiO_2	hydrated	polychromate	trichromate/tetrachromate	polychromate	—
	calcined	polychromate	—	polychromate	—
	reduced	$Cr^{2+}(Cr^{3+})$	—	strong reduced	Cr^{2+}
$Cr/SiO_2 \cdot Al_2O_3$ with 40 wt.% SiO_2	hydrated	chromate/polychromate	—	chromate	—
	calcined	chromate/polychromate	—	chromate	—
	reduced	$Cr^{2+/3+}$	—	less reduced	$Cr^{2+/3+}$
Cr/Al_2O_3	hydrated	chromate	dichromate/chromate	chromate	—
	calcined	chromate	—	chromate	—
	reduced	$Cr^{3+}(Cr^{2+})$	—	less reduced	Cr^{3+}

towards these species. In the reduced samples, Cr^{3+} gives no problem in DRS and EXAFS; on the other hand Cr^{2+} is only unambiguously detected by DRS and TPR, the latter indirectly *via* the average oxidation state.

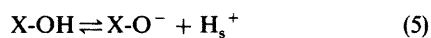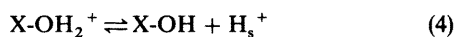## Chemistry of Chromium on Oxidic Surfaces

Hydrated Cr

In aqueous solution, the following pH-dependent equilibria can be envisaged:[37]

$$2CrO_4^{2-} + 2H^+ \rightleftharpoons Cr_2O_7^{2-} + H_2O \qquad (1)$$

$$\tfrac{3}{2}Cr_2O_7^{2-} + 2H^+ \rightleftharpoons Cr_3O_{10}^{2-} + H_2O \qquad (2)$$

$$\tfrac{4}{3}Cr_3O_{10}^{2-} + 2H^+ \rightleftharpoons Cr_4O_{13}^{2-} + H_2O \qquad (3)$$

The lower the aqueous solution pH, the more reactions (1)–(3) are driven to the right.

The hydroxy group population of an amorphous oxide[38] in contact with an aqueous solution is also subject to pH-dependent equilibria reactions:

$$X\text{-}OH_2^+ \rightleftharpoons X\text{-}OH + H_s^+ \qquad (4)$$

$$X\text{-}OH \rightleftharpoons X\text{-}O^- + H_s^+ \qquad (5)$$

$$H_s^+ \rightleftharpoons H^+ \qquad (6)$$

where $X = Si$ or Al, H_s^+ and H^+ are the surface and solution proton, respectively. $K_1 = [X\text{-}OH][H_s^+]/[X\text{-}OH_2^+]$, $K_2 = [X\text{-}O^-][H_s^+]/[X\text{-}OH]$ and the net pH at the isoelectric point $= (pK_1 + pK_2)/2$.

The isoelectric points (IEP) of the supports are summarized in Table 1 and increase from SiO_2 (2) over $SiO_2 \cdot Al_2O_3$ to Al_2O_3 (8). At low loadings, the surface of the oxide support determines the pH of the aqueous solution near the surface and, therefore, affects the equilibria (1)–(3). The lower the IEP of the support, the higher the H^+ concentration and the more these reactions are driven to the right (the more polymeric Cr oxide species exist in the aqueous film near the surface). Our DRS, RS and EXAFS spectra of the hydrated samples with small loadings agree with this model. Thus, SiO_2 is dominated by polychromate, alumina by chromate, while the $SiO_2 \cdot Al_2O_3$s have an intermediate chromate:polychromate ratio. When the loading increases two effects come into play: (1) the IEP is lowered owing to the presence of chromium, and decreases with increasing Cr loading; (2) the dispersion depends on the available surface area. Both factors influence the chemistry of chromium in the same direction, *i.e.* towards the formation of surface poly-chromates.

Anchored Cr

During calcination not only physisorbed water is removed, but also the polychromate species are anchored at the surface as evidenced by the consumption of OH groups (DRS), the decrease of the coordination number (EXAFS–XANES) and by direct IR investigations.[29] The anchoring process is an acid–base type reaction: the weaker acid H_2O is replaced by the stronger H_2CrO_4 (or $H_2Cr_2O_7$). The reaction is also support dependent as silica is more acidic than alumina. Thus, Cr^{6+} is more readily anchored to the surface of alumina, starting with the most basic OH groups and proceeding with the less basic ones, as the Cr loading increases. Therefore, Cr retains its atomic dispersion as monochromate up to loadings of *ca.* 4 wt.%. On hydrated silicas, mono- and poly-chromates are present at all loadings and the reaction with the hydroxy groups is insufficient to break the Cr clusters into monochromates. This is a problem both of strength

of interaction and of the density of OH groups. As Cr^{6+} is less dispersed on silica, calcination at 550°C gives partial conversion to Cr_2O_3 clusters. This is clearly evident in the DRS spectra and indirectly with EXAFS *via* the 2.05 Å Cr—O bond length, typical for Cr_2O_3. Such clusters become evident on alumina only at 8 wt.% Cr.

Reduced Cr

The Cr—O bond length of reduced samples (2.01–2.03 Å) are typical for Cr^{3+} in minerals.[39] On the basis of these bond lengths, a ligand-field parameter of 10 Dq = 16 700 ± 500 cm^{-1} is expected and indeed observed.[18,19] It also supports a (pseudo)octahedral coordination of Cr^{3+} on the surface of silica and alumina. However, our TPR and DRS studies reveal the presence of Cr^{2+}, especially on silica surfaces and low Cr loadings. The coordination numbers of 2.5 and 3.4 obtained by EXAFS on silica and alumina suggest that these $Cr^{3+/2+}$ ions are better described as coordinatively unsaturated species. This is in accordance with earlier IR results[12,40–44] on Philips catalysts, which show the presence of coordinative unsaturated Cr^{2+} ions on silica surfaces (*i.e.* Cr_A and Cr_B species). An overall reaction scheme could be:
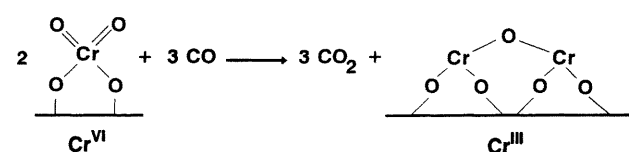
On silica this reaction proceeds further to Cr^{2+}:
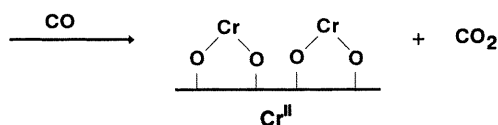
The reduction to Cr^{2+} is promoted at low loadings (Table 3), where a higher degree of dispersion of Cr is expected. Thus, at high loadings and low dispersion, reduction produces Cr_2O_3 and because this is the most stable oxide of Cr, reduction stops. At low loadings and high dispersion, migration of Cr^{3+} to form the stable Cr_2O_3 clusters is slow and reduction can continue to Cr^{2+}. The latter reduction step is favoured on silica which points to a strong Cr–support interaction. Silica is a chemically soft compound compared to alumina, because it facilitates electron fluctuations, necessary for reduction.[45] This property may explain also the difference in redox behaviour. Theoretical calculations are underway to substantiate this point.

Conclusions

By a combination of three spectroscopic techniques (DRS, RS and EXAFS–XANES) and one chemical technique (TPR) on the same set of samples, an overall picture of the surface chemistry of Cr emerges. (1) On hydrated surfaces the speciation of surface Cr depends on the isoelectric point of the support and Cr loading: the lower the isoelectric point and the higher the Cr loading, the more surface polychromates. (2) On calcined surfaces Cr oxides are anchored onto surface hydroxy groups and the speciation of surface Cr depends on the support composition and Cr loading: the higher the silica content of the support and the Cr loading, the more surface polychromates and Cr_2O_3. (3) On reduced surfaces Cr oxides are present as (coordinatively saturated and unsaturated) tri- and di-valent ions and their relative concentration is support and loading dependent: the $Cr^{2+} : Cr^{3+}$ ratio increases with increasing silica content and decreasing Cr loading.

References

1 M. P. McDaniel, *Adv. Catal.*, 1985, **33**, 47.
2 D. S. Kim, J. M. Tatibouet and I. E. Wachs, *J. Catal.*, 1992, **136**, 209.
3 F. D. Hardcastle and I. E. Wachs, *J. Mol. Catal.*, 1988, **46**, 173.
4 G. Deo and I. E. Wachs, *J. Phys. Chem.*, 1991, **95**, 5889.
5 M. A. Vuurman and I. E. Wachs, *J. Phys. Chem.*, 1992, **96**, 5008.
6 M. A. Vuurman, I. E. Wachs, D. J. Stufkens and A. Oskam, *J. Mol. Catal.*, 1993, **80**, 209.
7 M. A. Vuurman, F. D. Hardcastle and I. E. Wachs, *J. Mol. Catal.*, 1993, **84**, 193.
8 J. P. Hogan, *J. Polym. Sci.*, 1970, **8**, 2637; J. P. Hogan, in *Applied Industrial Catalysis*, Academic Press, New York, 1983, vol. 1, p. 149.
9 M. P. McDaniel, *J. Catal.*, 1981, **67**, 71; 1982, **76**, 17; 1982, **76**, 29; 1982, **76**, 37.
10 A. Zecchina, E. Garrone, G. Ghiotti, C. Morterra and E. Borello, *J. Phys. Chem.*, 1975, **79**, 966; 1975, **79**, 972; 1975, **79**, 978; 1975, **79**, 984.
11 H. L. Krauss, *Proceedings of the 5th International Congress on Catalysts, Palm Beach, 1972*, North-Holland, Amsterdam, 1973, vol. 1, p. 207; H. L. Krauss and H. Stach, *Z. Anorg. Allg. Chem.*, 1969, **366**, 280; H. L. Krauss, B. Rebenstorf and U. Westphal, *Z. Anorg. Allg. Chem.*, 1975, **414**, 97.
12 B. Rebenstorf and R. Larsson, *Z. Anorg. Allg. Chem.*, 1981, **478**, 119.
13 B. Fubini, G. Ghiotti, L. Stradella, E. Garrone and C. Morterra, *J. Catal.*, 1980, **66**, 200.
14 C. Groeneveld, P. P. M. M. Wittgen, A. M. van Kersbergen, P. L. M. Hestrom, C. E. Nuijten and G. C. A. Schuit, *J. Catal.*, 1979, **59**, 153.
15 N. E. Fouad, H. Knözinger, M. I. Zaki and S. A. A. Mansour, *Z. Phys. Chem.*, 1991, **171**, 75.
16 N. E. Fouad, H. Knözinger, H. M. Ismail and M. I. Zaki, *Z. Phys. Chem.*, 1991, **173**, 201.
17 N. E. Fouad, H. Knözinger and M. I. Zaki, *Z. Phys. Chem.*, 1994, **186**, 231.
18 B. M. Weckhuysen, L. M. De Ridder and R. A. Schoonheydt, *J. Phys. Chem.*, 1993, **97**, 4756.
19 B. M. Weckhuysen, A. A. Verberckmoes, A. L. Buttiens and R. A. Schoonheydt, *J. Phys. Chem.*, 1994, **98**, 579.
20 B. M. Weckhuysen, L. M. De Ridder, P. J. Grobet and R. A. Schoonheydt, *J. Phys. Chem.*, 1995, **99**, 320.
21 B. M. Weckhuysen, I. E. Wachs and R. A. Schoonheydt, *Stud. Surf. Sci. Catal.*, 1995, **91**, 151.
22 B. M. Weckhuysen, H. J. Spooren and R. A. Schoonheydt, *Zeolites*, 1994, **14**, 450.
23 B. M. Weckhuysen and R. A. Schoonheydt, *Stud. Surf. Sci. Catal.*, 1994, **84**, 965.
24 A. I. Frenkel, E. A. Stern, M. Qian and M. Newville, *Phys. Rev. B*, 1993, **48**, 12449.
25 J. J. Rehr, R. C. Albers and S. I. Zabinski, *Phys. Rev. Lett.*, 1992, **69**, 3397.
26 M. Newville, P. Livins, Y. Yacoby, J. J. Rehr and E. A. Stern, *Phys. Rev. B*, 1993, **47**, 14146.
27 B. K. Teo, *EXAFS: Basic Principles and Data Analysis*, Springer-Verlag, New York, 1986.
28 J. M. Jehng, I. E. Wachs, B. M. Weckhuysen and R. A. Schoonheydt, *J. Chem. Soc., Faraday Trans.*, 1995, **91**, 953.
29 A. M. Turek, I. E. Wachs and E. De Canio, *J. Phys. Chem.*, 1992, **96**, 5000.
30 L. K. Przhevalkaya, V. A. Shvets and V. B. Kazanskii, *Kinet. Katal.*, 1970, **11**, 1310.
31 A. Cimino, B. A. De Angelis, A. Luchetti and G. Minelli, *J. Catal.*, 1976, **45**, 316.
32 G. Ghiotti, E. Garrone, G. Della Gatta, B. Fubini and E. Giamello, *J. Catal.*, 1983, **80**, 249.
33 L. A. Grunes, *Phys. Rev. B*, 1983, **27**, 2111.
34 S. Bordiga, F. Bosherini, S. Coluccia, F. Genoni, C. Lamberti, G. Leofanti, L. Marchese, G. Petrini, G. Vlaic and A. Zecchina, *Catal. Lett.*, 1994, **26**, 195.
35 J. Wong, F. W. Lytle, R. P. Messmer and D. H. Maylotte, *Phys. Rev. B*, 1984, **30**, 5596.
36 M. V. Twigg, *Catalyst Handbook*, Wolfe, London, 2nd edn., 1989; C. L. Thomas, *Catalytic Processes and Proven Catalysts*, Academic Press, New York, 1970.
37 N. N. Greenwood and A. Earnshaw, *Chemistry of the Elements*, Pergamon Press, Oxford, 1984.
38 G. A. Parks, *Chem. Rev.*, 1965, **65**, 177.
39 R. G. Burns, *Mineralogical Applications of Crystal Field Theory*, Cambridge University Press, Cambridge, 2nd edn., 1993.
40 G. Ghiotti, E. Garrone and A. Zecchina, *J. Mol. Catal.*, 1988, **46**, 61.
41 G. Ghiotti, E. Garrone and A. Zecchina, *J. Mol. Catal.*, 1988, **65**, 73.
42 A. Zecchina, G. Spoto, G. Ghiotti and E. Garrone, *J. Mol. Catal.*, 1994, **86**, 423.
43 G. Spoto, S. Bordiga, E. Garrone, G. Ghiotti and A. Zecchina, *J. Mol. Catal.*, 1992, **74**, 175.
44 C. S. Kim and S. I. Woo, *J. Mol. Catal.*, 1992, **73**, 249.
45 B. G. Baekelandt, W. J. Mortier and R. A. Schoonheydt, *Struct. Bond.*, 1993, **80**, 187.